water

MDPI

Article

Influence of Airfoil Curvature and Blade Angle on Vertical Axis Hydraulic Turbine Performance in Low Flow Conditions

Chunyun Shen [1], Yubing Han [1], Shiming Wang [1,*] and Zekun Wang [2,*]

[1] College of Engineering Science and Technology, Shanghai Ocean University, Shanghai 201306, China; cyshen@shou.edu.cn (C.S.); hanyubing2033@foxmail.com (Y.H.)
[2] School of Mechatronic Engineering and Automation, Shanghai University, Shanghai 200444, China
* Correspondence: smwang@shou.edu.cn (S.W.); zkwang@shu.edu.cn (Z.W.)

Abstract: The vertical axis hydrokinetic turbine is increasingly being used as a renewable energy device to harness tidal energy. In coastal regions with low tidal flow velocities, vertical-axis hydrokinetic turbines often exhibit low energy conversion efficiency, limiting their engineering applications. However, research in this field lacks systematic reviews and reliable solutions for improving efficiency. The paper, based on the traditional vertical axis hydrokinetic turbines, utilized numerical calculations and experimental methods to investigate the effects of blade helicity and airfoil curvature on the energy conversion efficiency of vertical axis hydrokinetic turbines in low flow velocity conditions. Additionally, an improved vertical-axis turbine model is proposed to enhance energy conversion efficiency in low-flow environments. The results indicate that increasing the blade helical angle and airfoil curvature can better optimize the flow conditions around the turbine, significantly improving the energy conversion efficiency of vertical axis turbines. The airfoil blade with a 20% curvature performs best at blade angle, with its power coefficient curve reaching higher peak values at several azimuth angles. At this point, the maximum efficiency reaches 24.42%. Compared to the conventional straight-blade design, the improved turbine model exhibits 6.13% increase in average energy capture efficiency, 3.70% increase in average dynamic torque, and 11.1% improvement in self-starting performance. Comparative analysis reveals that vertical-axis helical blade turbines exhibit superior hydrodynamic performance under low-flow conditions, effectively overcoming the limitations of conventional straight-blade turbines, including poor self-starting capability and low efficiency. This research provides valuable insights into improving the performance of vertical-axis turbines in low-flow environments and suggests innovative solutions for optimizing turbine design.

Keywords: vertical axis hydraulic turbine; numerical simulation; low flow velocity; power coefficient; self-starting capability

Academic Editor: Chin H Wu

Received: 22 October 2024
Revised: 15 December 2024
Accepted: 20 December 2024
Published: 24 December 2024

Citation: Shen, C.; Han, Y.; Wang, S.; Wang, Z. Influence of Airfoil Curvature and Blade Angle on Vertical Axis Hydraulic Turbine Performance in Low Flow Conditions. *Water* **2025**, *17*, 11. https://doi.org/10.3390/w17010011

1. Introduction

Hydropower, as a clean and renewable energy source, has garnered significant attention, with tidal energy generation becoming a prominent focus of research [1]. Vertical axis turbines, which convert the kinetic energy of water flow into mechanical energy, have been extensively utilized in renewable energy applications, including rivers and oceans [2]. Traditional tidal current power generators are typically deployed in specific regions where water flow speeds exceed 2–3 m/s [3]. However, for most coastal regions characterized by low flow velocities, it is particularly important to develop power generation devices specifically designed for low-velocity tidal currents, thereby improving

their applicability [4]. The Darrieus-type vertical axis turbine, characterized by its rotor axis being perpendicular to the flow direction and operating based on the fluid lift, has been extensively utilized in the wind energy sector [5]. This type of turbine features a simple structure, is insensitive to flow direction, is easy to install, and maintains relatively high energy conversion efficiency under low-flow velocity conditions [6,7]. Additionally, they can be arranged in arrays to efficiently concentrate and capture energy [8]. As the core device for capturing and converting kinetic energy from water, the performance of vertical-axis hydrokinetic turbines directly influences the efficiency of water kinetic energy conversion. Conventional straight bladed vertical axis water turbines face several limitations, including the inability to self-start under load, unstable operation, susceptibility to stalling, and low efficiency. Enhancing the energy capture efficiency of vertical axis hydrokinetic turbines under low flow conditions remains a key area of research. The study identified solidity [9], blade shape [10], helicity [11], airfoil profile, and the design of connecting rods [12] as the primary parameters influencing the energy conversion efficiency of vertical axis turbines. Dendy Satrio [13] improved the energy conversion efficiency of vertical axis turbines under low-flow velocity conditions by introducing flow bypass structures, whereas Furhan Khan [14] achieved similar enhancements using variable pitch methods. Although these solutions are effective, they increase the structural complexity of the turbine, thus undermining its inherent advantage of simplicity. Gharib Yosry [15] investigated the impact of free surface variation on the energy conversion efficiency of micro vertical-axis turbines under low-flow velocity conditions, observing that in such conditions, a higher solidity can enhance the turbine's energy conversion efficiency. Abdolahifar [16] optimized traditional straight blades into V-shaped blades and observed that their energy conversion efficiency was lower than that of traditional straight blades at high tip-speed ratios (TSR), while at low TSR, their efficiency was inferior to that of helical blades. Peter Bachant [17] compared spherical Lucid blades with cylindrical helical Gorlov blades and concluded that the Gorlov Helical Turbine (GHT) offers superior energy conversion efficiency. Under low flow velocity conditions, maintaining high energy conversion efficiency while improving the self-starting capability of vertical axis water turbines is another key focus of research [18]. To address this issue, researchers have combined Savonius and Darrieus rotors, integrating lift and drag blades to enhance the self-starting performance of vertical axis turbines [19–21]. Although this combination improved self-starting characteristics, it reduced energy conversion efficiency. To maintain a high energy conversion rate, Dendy Satrio [22] found that adjusting the tilt angles of vertical-axis blades and ensuring a reasonable blade distribution can enhance starting torque at various azimuth angles, thereby improving self-starting capability. Building on this foundation, Parag K. Talukdar [23] and Sathit Pongduang [24] conducted experiments with NACA0020 airfoils featuring blades with varying helical angles, evaluating energy conversion efficiencies at different tip-speed ratios and helical angular velocities. The helical configuration of the blades along their rotational trajectory ensures that specific sections of the blade profile consistently maintain an optimal angle of attack, thereby effectively harnessing the incoming flow forces. Compared to conventional straight blade vertical axis turbines, this design enables smoother operation and produces more uniform torque, thereby significantly improving the self-starting performance of the hydrokinetic turbine [25]. Moreover, adjusting the blade's helical angle neither incurs additional design costs nor introduces structural complexity to the vertical axis turbine. Currently, the majority of airfoil designs for helical vertical axis hydrokinetic turbines predominantly employ symmetrical airfoils. However, asymmetric airfoils, due to their unique geometry, can achieve higher lift coefficients at the same angle of attack, thereby improving energy capture efficiency. Jiahao Zhang [26] employed a surrogate modeling approach to elucidate

the relationship between turbine performance, airfoil shape, and flow characteristics under low-flow velocity conditions. B. Yang [27] applied a genetic algorithm to optimize the symmetric NACA0012 airfoil, and the results demonstrated that the optimized asymmetric airfoil exhibited superior hydrokinetic performance.

Previous studies have identified the primary design challenges of vertical-axis water turbines to be the selection of airfoil parameters and the structural design of the blades. The influence of various turbine parameters on performance is intricate and highly interdependent. Most prior research has predominantly focused on the effects of individual variables, such as blade shape or airfoil profile, on the hydrokinetic performance of vertical-axis turbines. However, comprehensive and systematic analyses of the effects of airfoil design and helical blade configurations on hydrokinetic performance and energy efficiency under low-flow velocity conditions remain limited. The research utilizes a combined approach of numerical simulation and experimentation to examine the hydrokinetic performance of a vertical axis turbine equipped with airfoil blades at varying helical angles under low-flow velocity conditions. The effects of various airfoil designs and blade helical configurations on the energy conversion efficiency and self-starting performance of the turbine are analyzed. The findings of this research offer valuable references and guidance for optimizing the performance of vertical-axis water turbines in low-flow velocity environments.

2. The Model and Methods

2.1. The Vertical Axis Turbine Model

Offshore tidal current turbines are widely distributed in medium and low speed tidal current zones (below 1 m/s). The paper first conducts a simulation analysis of the hydrokinetic performance of vertical axis tidal turbines under low flow velocity conditions.

Select a flow velocity of 0.8 m/s for the simulation experiment. The vertical axis turbine model as shown in Figure 1.

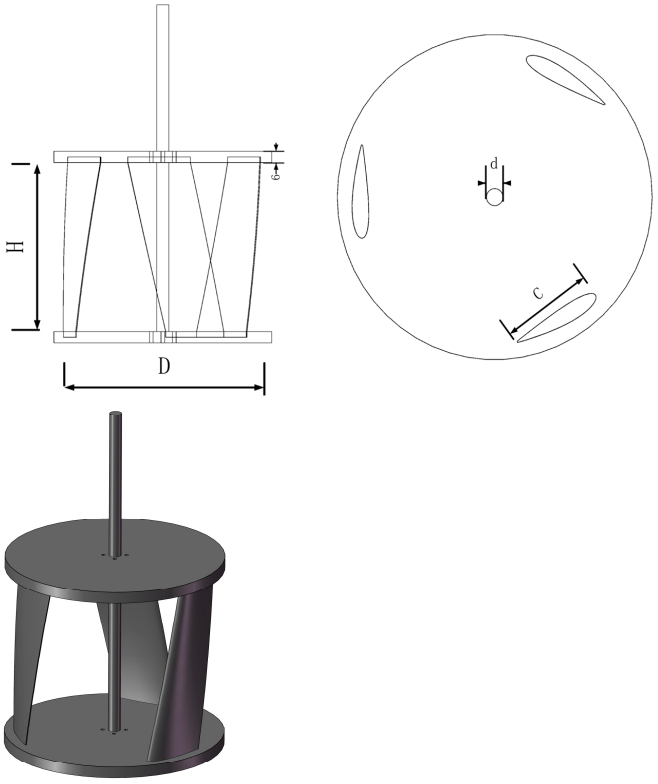

Figure 1. Structure of the Vertical Axis Hydrokinetic Turbine.

The blade airfoil shape is a key focus in research on vertical-axis hydraulic turbines, aiming to enhance energy conversion efficiency. By selecting different airfoil shapes, the energy conversion efficiency and self-starting performance of the turbine can be effectively enhanced under varying flow velocity conditions. The NACA four-digit series airfoils are commonly used in vertical axis turbines due to their simple design and excellent hydrokinetic performance in water [28]. The NACA four-digit airfoil series is defined as follows: the first digit represents the maximum curvature as a percentage of the chord length, the second digit indicates the position of the maximum curvature relative to the leading edge, and the last two digits represent the maximum thickness of the airfoil as a percentage of the chord length. The selected blade airfoils are NACA0018, NACA2418, and NACA4418, as shown in Figure 2. All three airfoils share the same maximum thickness, while their relative curvatures differ.

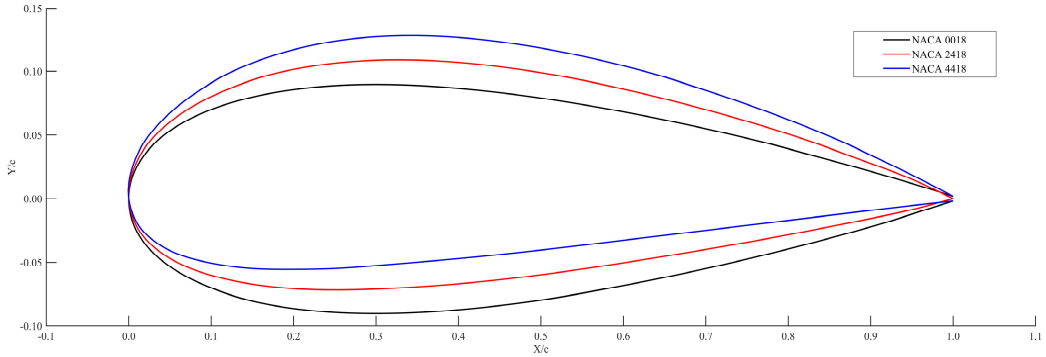

Figure 2. The different airfoil curvatures of blade profiles.

The aspect ratio [29] (height-to-diameter ratio)

$$\sigma = \frac{nC}{R}$$

where n is the number of blades, C is the blade chord length, and R is the turbine radius.

The ratio of blade height to rotor radius (aspect ratio) affects the Reynolds number, which in turn affects starting torque and energy conversion efficiency. For small turbines, an aspect ratio of 0.2 m for height and diameter selection provides the best performance and highest tip speed ratio [30]. The chord length was set to 0.07 m, resulting in a high solidity of σ = 2.1. and the pitch angle is 0°. The overall design parameters of the vertical axis turbine are shown in Table 1.

Table 1. Structure and overall design parameters of the Vertical Axis Hydrokinetic Turbine.

Structural Parameters	Values	Structural Parameters	Values
Blade Type (NACA)	0018/2418/4418	Helicity (λ)	$0^\circ/30^\circ/60^\circ/90^\circ$
Inflow velocity	0.8 m/s	Water flow density	1000 kg/m^3
Diameter (D)	0.2 m	Blade chord length (C)	0.07 m
Number of blades (n)	3	Blade height (H)	0.2 m
pitch angle (β)	0°		

λ is the blade helicity, indicating the degree of wrap of the blades on the cylindrical surface of the vertical axis turbine.

$$\lambda = \frac{n\alpha}{360^\circ}$$

where n is the number of blades, and α is the angle formed between the projection of the blade tip on the base and the blade at the base. The turbine combined with helical blades is a vertical axis helical turbine, and a straight blade vertical turbine can be considered as a vertical axis helical turbine with a helix angle of 0°, as shown in Figure 3.

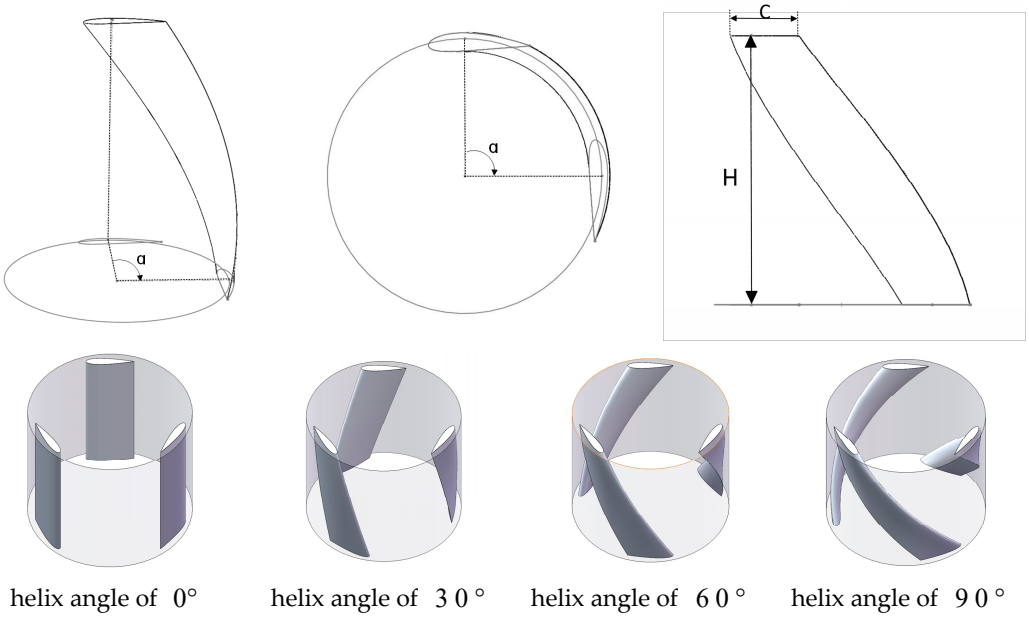

Figure 3. The blade helical model.

The main performance parameters of a vertical axis hydrokinetic turbine include the power coefficient C_p, Torque coefficient C_m, Tip speed ratio (TSR).

The power coefficient represented the ratio between the turbine's output power and the fluid's kinetic energy at a given flow velocity. It served as a key indicator of turbine performance, and its expression is:

$$C_p = \frac{\omega T}{\frac{1}{2}\rho V_0^2 A} = C_m \cdot TSR \tag{1}$$

where ρ is the water density, kg/m^3, V_0 is the incoming flow velocity, measured in meters per second (m/s). A is the interface of the turbine's rotational domain ($A = D \cdot H$).

ω is the rotational speed of the rotor, $\omega = \int \frac{T-f}{F} dt$.

The forces acting on the vertical axis turbine were analyzed based on Newton's second law:

$$T = F\frac{d\omega}{dt} + f$$

where T is the total torque on the turbine blade; F is the moment of inertia of the turbine, and f is the load torque.

The torque coefficient C_m is used to quantify and optimizes the start-up performance, operational stability and overall efficiency of the vertical axis turbine with the expression:

$$C_m = \frac{T}{\frac{1}{2}\rho V_0^2 DA} \tag{2}$$

The tip speed ratio (TSR) is defined as the ratio of the blade tip's linear velocity to the incoming flow velocity.

$$TSR = \frac{\omega R}{V_0} \tag{3}$$

The hydrokinetic forces on the vertical axis turbine blades during rotation produced varying torques depending on the angle of attack, causing periodic fluctuations in the power coefficient with the azimuthal angle. Therefore, the average energy capture coefficient over one motion cycle was introduced for the turbine.

$$\overline{C_p} = \frac{1}{t}\int_0^t C_p \cdot dt \tag{4}$$

where t is the time required for the turbine to complete one operational cycle.

Parameter δ was introduced to measure the instability of power output.

$$\delta = \frac{C_{p_{\max}} - C_{p_{\min}}}{\overline{C_p}} \tag{5}$$

where $C_{p_{\max}}$ and $C_{p_{\min}}$ are the maximum and minimum power coefficients of the turbine in a rotation cycle, respectively, reflecting the degree of power fluctuation during operation. The smaller the value of degree of power fluctuation, the smoother the operation of the vertical axis turbine.

2.2. Methods

The fluid was liquid water, and the incompressible fluid momentum equation used in the simulation can be expressed as:

$$\rho(\frac{\partial u}{\partial t} + u \cdot \nabla u) = -\nabla p + \mu\nabla^2 + f_0$$

where ρ is the water density, p is the pressure exerted on the fluid element, μ is the velocity vector.

The energy equation can be expressed as:

$$\frac{\partial T}{\partial t} + \varphi \cdot \nabla T = \alpha\nabla^2 T + Q$$

where T is the temperature, φ is the fluid velocity vector, α is the thermal diffusivity, and Q is the internal energy.

Based on the vertical axis hydraulic turbine model selected for the paper, 3D transient analyses have been carried out using ANSYS FLUENT (2021) software, and a double-precision model is selected. To address issues involving boundary layers and complex flow conditions, the SST k-ω turbulence model was selected. This model is well-suited for handling turbulent flow near walls and accurately simulates shear stress and turbulent viscosity effects in the near-wall region. It is particularly applicable to low Reynolds number and low-speed flow models.

All simulations used the COUPLED pressure and velocity solved method. Second-order upwind schemes were applied to the equations for momentum, turbulent kinetic energy, and specific dissipation rate, while second-order discretization was similarly used for the pressure equations. The software solves the flow-governing equations using the least squares cell-based gradient technique for spatial discretization. In each time step, convergence criteria were established with a threshold of 10^{-5} for the residuals of all momentum, continuity and turbulence equations. The dynamic mesh and 6-DOF passive rotation techniques were employed [31]. The system load is applied via the system damping

constant to support the analysis of rigid object motion. The 6-DOF solver calculates the hydrokinetic moment by integrating surface pressure and shear stress on the turbine blade, which is then used to determine the motion of the rigid object. By applying the optimal simulation load, the turbine's flow behavior during passive rotation driven by water flow was obtained and analyzed [32]. During the simulation process, the turbine blade was subjected to the combined effects of the hydrokinetic moment, inertia moment, and damping moment acting on the turbine, causing it to rotate around the Z-axis at a rotational speed. This numerical simulation method can more accurately replicate the actual operating state of the turbine while enabling the measurement of the torque generated by the kinetic energy of the water flow during rotor startup.

2.3. Mesh Independence Verification

The computational fluid domain model was divided into two parts: a rotating domain for the rotor and a fluid domain. The inlet flow velocity for the fluid domain was set to 0.8 m/s, while the outlet was defined using a pressure outlet boundary condition. The rotational region utilizes an overlapping mesh approach to seamlessly transfer data and boundary conditions between the stationary and rotating domain meshes. This method enables the fluid medium to flow smoothly from the inner rotating region to the outer rotating region through the overlapping grid technique. The mesh generation is shown in Figure 4.

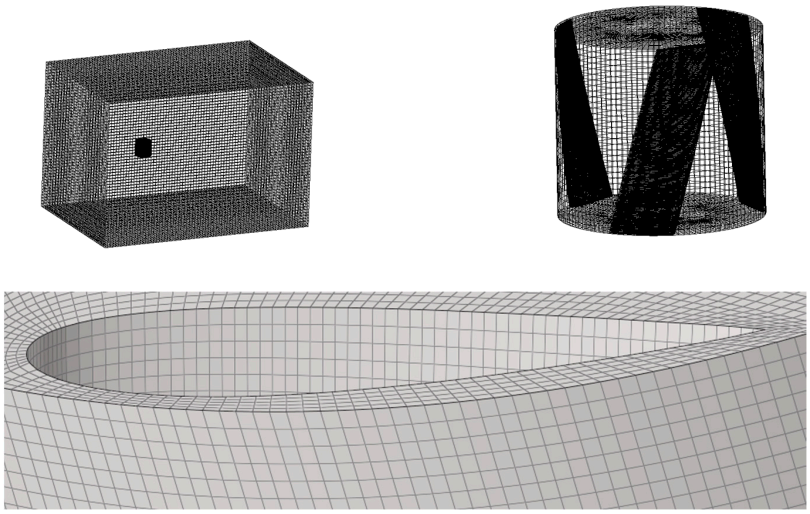

Figure 4. Computational grid.

Grid generation is a fundamental aspect of computational fluid dynamics, as grid density significantly impacts the accuracy of computational results. An appropriate grid count effectively reduces computational time and costs while ensuring satisfactory simulation accuracy. The grid refinement process was conducted using Roache's Grid Convergence Index (GCI), a method based on the generalized Richardson extrapolation. It involves comparing the discrete solutions from two different grid spacings. The torque coefficient was used as the reference value, with a recommended safety factor of 1.25, and the calculated convergence value was 3.0. The dimensionless distance of the first layer from the wall determines the mesh quality. The boundary layer over the turbine blades characterizes the flow surrounding the turbine. The computational domain was discretized using a fully structured mesh composed of hexahedral cells. Mesh refinement was focused around the turbine blade and within the rotational domain. The height of the first mesh layer near the blade was adjusted to ensure $y^+ < 1$ was satisfied. In the research, numerical calculations were performed on four models with different mesh densities [33]. The specific parameters are shown in Table 2.

Table 2. Influence of time step and mesh on power output.

Number	Rotating Domain	Total Number	Torque Coefficient	Error	GCI	Refinement Factor
1	462,803	976,450	0.204	-	-	0.5
2	891,731	1,405,378	0.159	28.3%	8.44%	1
3	1,631,242	2,624,973	0.186	14.47%	3.03%	2
4	2,840,799	3,834,530	0.182	2.2%	0.38%	4

Figure 5 shows the results obtained for different rotation angles/time step values. A time step sensitivity analysis was performed using a mesh with 2,624,973 grid points. The time step in FLUENT was adjusted based on the time required for one complete rotation of the turbine and the rotational angular velocity obtained from the 6-DOF passive rotation simulator. In the research, the rotational angular velocities of the 12 turbines under optimal load conditions are not the same; therefore, the angular displacement per second of the turbines will be used as the standard for the time step. In the transient simulation when the rotation angle/time step was reduced below 2°/time step, the impact on accuracy became negligible (with an error of 0.29% at 1°). A total grid count of 2,624,973 and a 2°/time step were chosen as the optimal balance between accuracy and computational time cost.

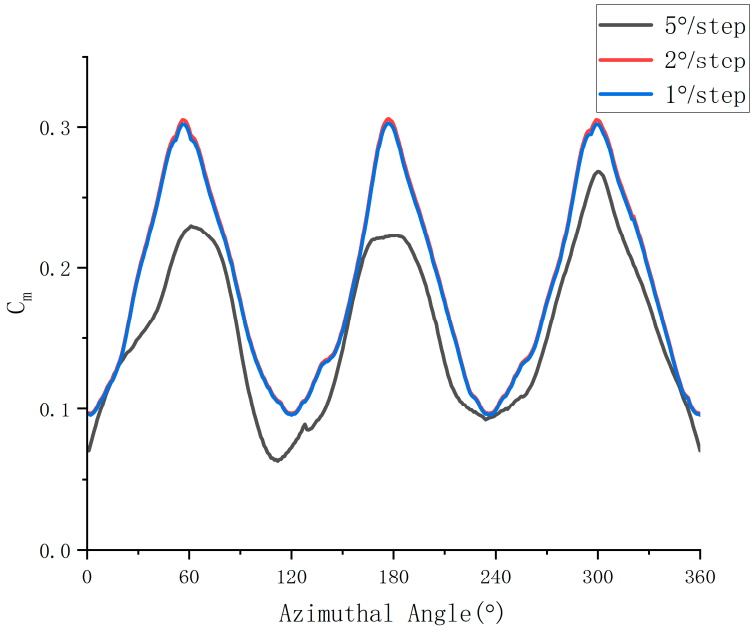

Figure 5. Torque coefficient for different time-steps.

3. Results and Discussions

3.1. The Influence of Airfoil Curvature and Blade Twist on Energy Conversion Efficiency

The energy conversion efficiency of vertical axis turbines is an indicator that quantifies the efficiency with which fluid kinetic energy is transformed into mechanical energy. The efficiency is typically expressed by the power coefficient, reflecting the turbine's energy conversion capability under various operating conditions. Variations in flow velocity and blade design significantly impact turbine performance, especially in low flow velocity. Twelve turbine models were designed and simulated, incorporating three different airfoil curvatures and four distinct blade helical angles. The variation of the power coefficient of the vertical axis turbine with the azimuthal angle was obtained, as shown in Figure 6.

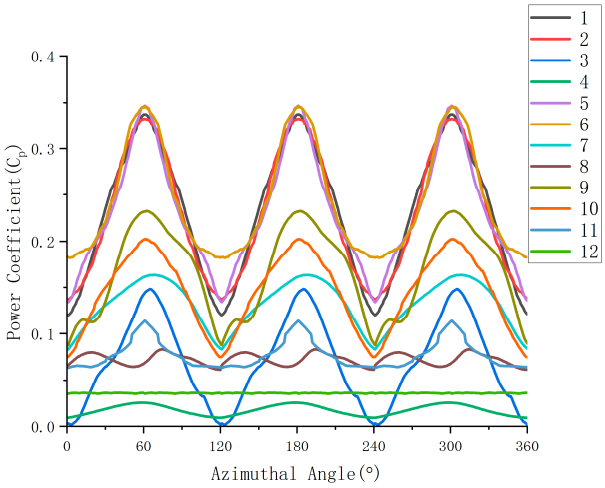

Figure 6. The power coefficient with different blade helical angles and airfoil curvatures.

The power coefficient of some turbines exhibited distinct periodic fluctuations within one rotation cycle, demonstrating the variation pattern of the power output of vertical axis turbines. This periodicity is determined by the structural characteristics of the turbine. As the rotor rotates, the relative position of the blades in the incoming flow continuously changes, causing the power coefficient of the vertical axis turbine to exhibit periodic variation. The torque values of the turbine over one rotation cycle were obtained through simulations, and the average power of different vertical axis turbines was calculated according to Equation (4) as shown in Table 3. The fluctuation rate was also determined from these results. The results indicated that the airfoil shape significantly impacted the turbine's energy conversion efficiency. Blades with a 20% curvature airfoil performed best at a helical angle 30°, with the power coefficient curve reaching higher peaks at several azimuth angles. The overall power coefficient remained relatively high, and the average power reached 24.42%. Compared to the symmetric airfoil turbine without blade twist, its average energy conversion efficiency increased by 6.13%. According to Equation (5), the fluctuation rate of the vertical axis turbine was calculated. It was found that the original straight-blade NACA0018 had a fluctuation rate of 94.74%, while the NACA2418 blade with 30° had a fluctuation rate of 64.29%, representing a reduction of 32.14%. As the helical angle increases, the fluctuation in the blades' dynamic torque decreases. This indicates that the helical modification leads to a more uniform hydrokinetic force distribution on the blades. This design reduces torque pulsation and enhances the self-starting ability.

Table 3. The power coefficient and overall design parameters of vertical axis water turbines with blade helical angles and airfoil curvatures.

Number	Airfoil	Helical Angle	Power Coefficient
1	NACA0018	0°	23.01%
2		30°	23.26%
3		60°	5.67%
4		90°	1.75%
5	NACA2418	0°	23.32%
6		30°	24.42%
7		60°	12.57%
8		90°	7.24%
9	NACA4418	0°	18.63%
10		30°	15.10%
11		60°	6.18%
12		90°	3.59%

Moderately increasing the airfoil curvature and blade helical angle can enhance the energy conversion efficiency of vertical axis turbines, as shown in Figure 7a,b. At low flow velocity conditions, different airfoil curvatures have varying effects on energy conversion from the water flow, as shown in Figure 7c–e. However, further increasing the airfoil curvature and blade helical angle can actually reduce the energy conversion efficiency of the turbine. In addition, under the 90° helical angle configuration, the energy conversion efficiency of the three turbine models was relatively low, indicating that an excessively large helical angle may negatively affect the hydrokinetic performance of vertical axis turbines. An appropriate helical angle can optimize the blade's hydrokinetic performance throughout the entire rotation, thereby improving energy conversion efficiency.

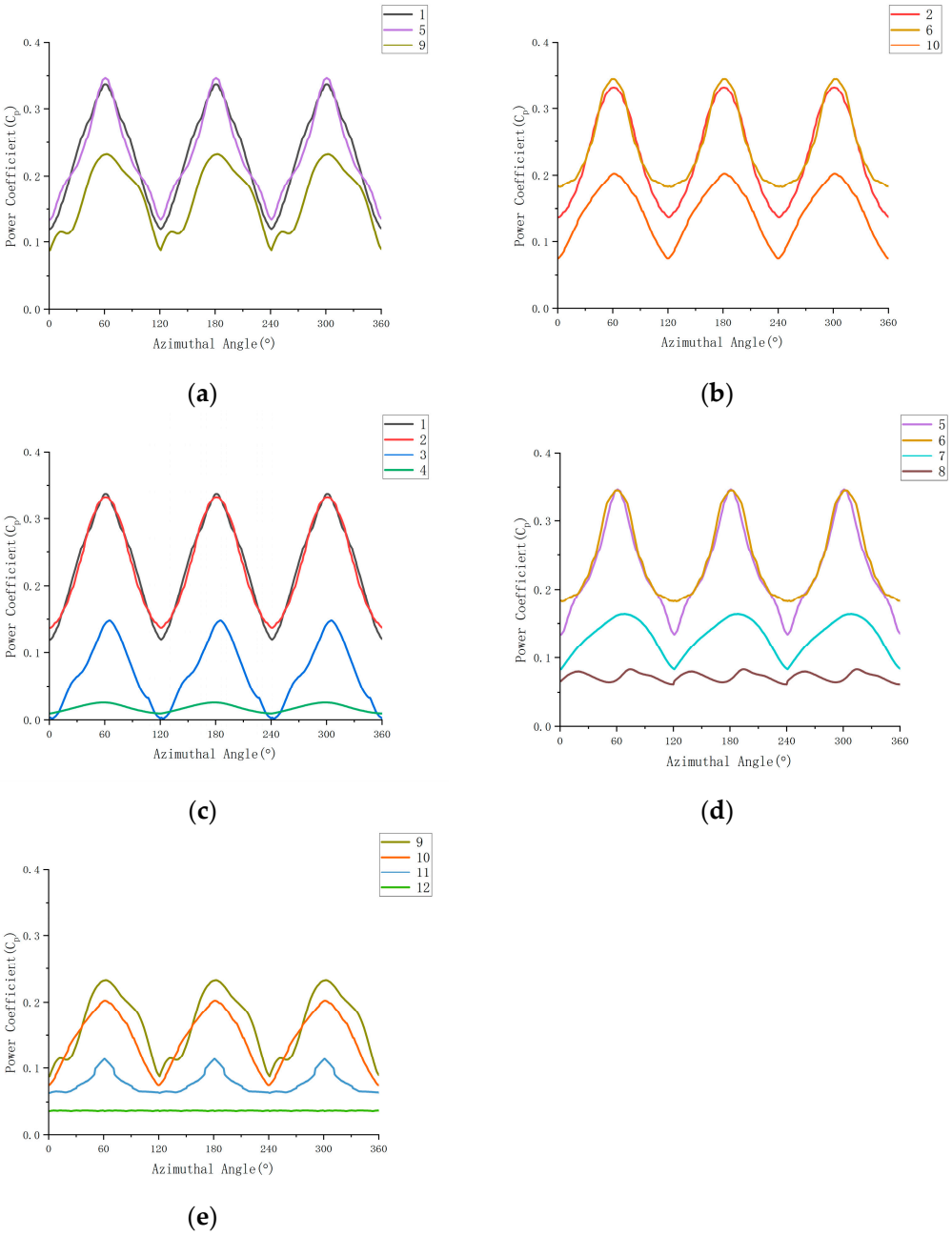

Figure 7. The power coefficient curves of turbines with different airfoil profiles and helicity. (**a**) Blades with the 0% 20% 40% curvature at a helical angle of 0°; (**b**) Blades with the 0% 20% 40% curvature at a helical angle of 30°; (**c**) Blades with a 0% curvature at helicity angle of 0°, 30°, 60°, 90°; (**d**) Blades with a 20% curvature at a helicity angle of 0°, 30°, 60°, 90°; (**e**) Blades with a 40% curvature at a helicity angle of 0°, 30°, 60°, 90°.

3.2. Analysis of the Effects of Airfoil Curvature and Blade Twist on the Hydrokinetic Performance of Turbines

Figure 8 illustrates the velocity contours of the turbine at different vertical positions. The findings indicate that variations in blade design significantly impact the flow field surrounding the turbine, leading to changes in the force distribution on the blade surface. The upper section shows the turbine with a symmetric airfoil (NACA0018) and 0°, while the lower section displays the turbine with an asymmetric airfoil (NACA2418) and 30°. During one rotation cycle, the straight blade experiences significant velocity fluctuations. In contrast, the velocity along the span of the helical blade is relatively uniform providing greater lift force to the blades. Figure 9 illustrates the velocity vector diagram of the turbine cross-section. By comparing the flow field velocity characteristics of the symmetric and asymmetric airfoils under low flow velocity, it can be observed that flow separation occurs on both the downstream and upstream sides of the blade. This is characterized by the fluid detaching from the main flow path along the airfoil surface. In contrast, the asymmetric airfoil (NACA2418) at specific helical angles is able to better optimize the flow field. This design promotes better fluid adherence to the blade surface, reduces the adverse effects of flow separation and turbulence, and enhances energy conversion efficiency.

The flow velocity along the centerline of the internal flow field, as shown in Figure 10, exhibits significant fluid disturbances and velocity fluctuations within the vertical axis turbine. In comparison, the straight blades with 0° produced more intense flow disturbances and velocity fluctuations, while the asymmetric twisted blades exhibited a smoother flow field and more stable velocity distribution. Under low flow velocity conditions, the asymmetric blades demonstrated higher stability. The flow separation and reattachment phenomena on the asymmetric blades are more uniform, and this uniformity and regularity help reduce periodic torque fluctuations, thereby enhancing the overall stability of the turbine.

Figure 11 illustrates the pressure contour of the turbine, where the pressure distribution exhibits periodic changes as the blade angle varies. A high-pressure region formed on the windward side of the blade, while a low-pressure region appeared on the leeward side. Additionally, we analyzed the pressure on the windward surface of the blade. Figure 12 illustrates the variation in the area-averaged pressure on the windward side throughout the rotation cycle. In comparison, the pressure distribution on the asymmetric twisted blades is more stable, with smaller disturbances. This reduces the fluctuation rate during the vertical axis turbine's rotation cycle, thereby improving the overall energy conversion efficiency of the turbine. The asymmetric twisted airfoil has a larger curvature on the upper surface, which accelerates the flow over it, leading to a pressure drop. This generates significant lift at relatively small angles of attack while maintaining good lift performance over a wide range of attack angles. It effectively alleviates flow separation on the airfoil surface, suppresses vortex formation, and reduces induced drag. The rotational flow induced by the helical blades increases the added angular momentum, thereby improving energy capture efficiency.

Under low flow conditions, the flow state within the turbine often exhibits nonlinear dynamics, resulting in unstable and highly variable hydrodynamic performance. Future research will focus on further exploring the mechanisms influencing these hydrodynamic behaviors.

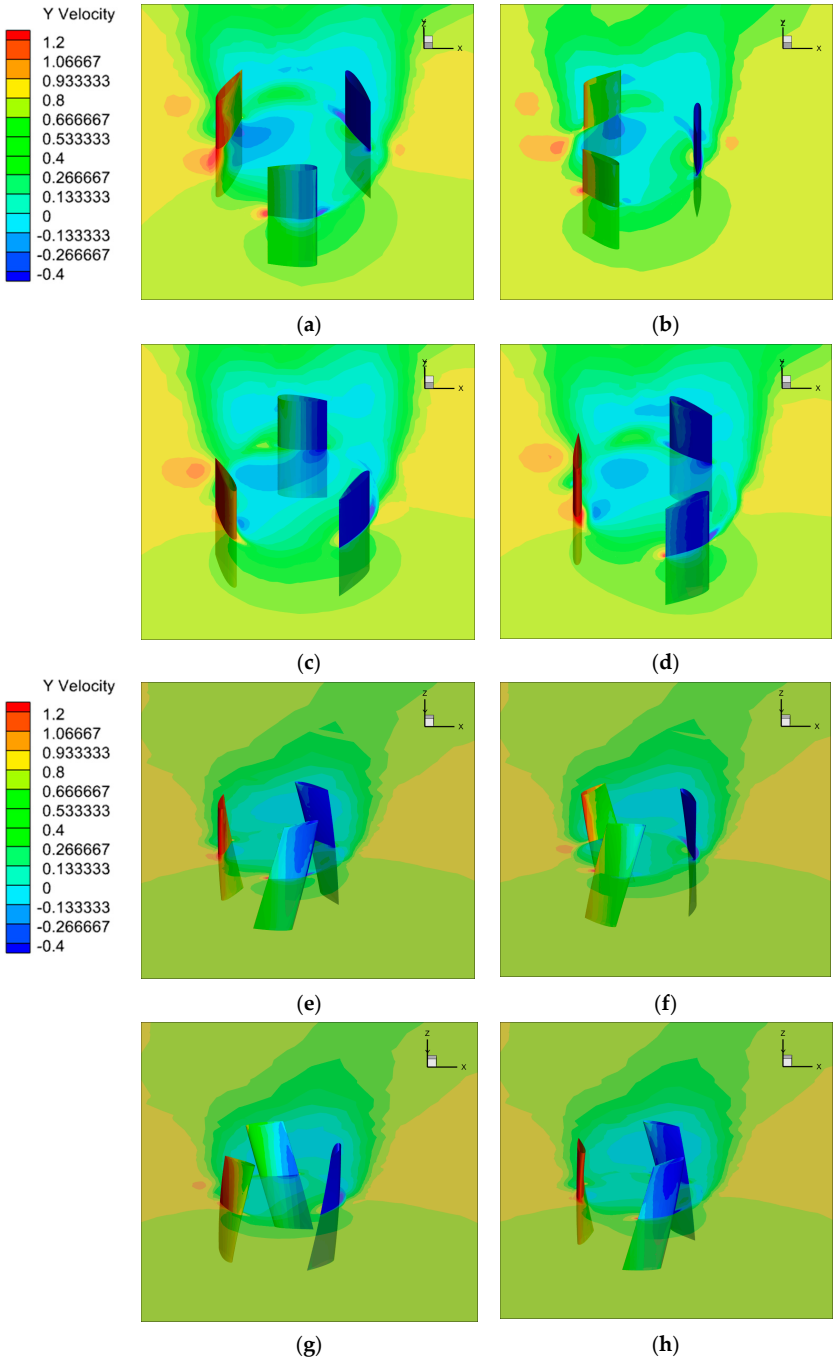

Figure 8. The flow characteristics at different blade rotation positions. (**a**) $\theta = 0°$; (**b**) $\theta = 30°$; (**c**) $\theta = 60°$; (**d**) $\theta = 90°$; (**e**) $\theta = 0°$; (**f**) $\theta = 30°$; (**g**) $\theta = 60°$; (**h**) $\theta = 90°$.

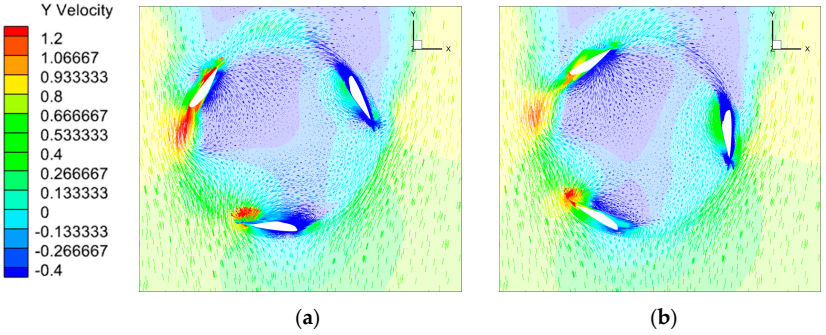

Figure 9. *Cont.*

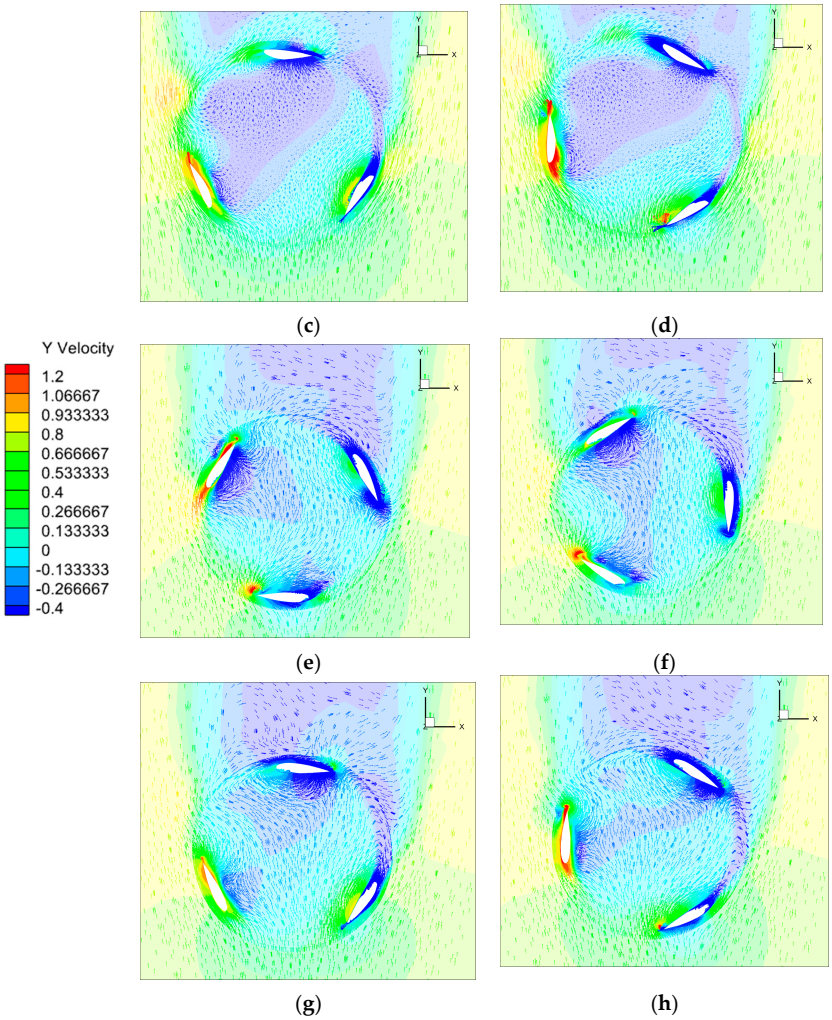

Figure 9. Velocity vector plot of turbine airfoils. (**a**) $\theta = 0°$; (**b**) $\theta = 30°$; (**c**) $\theta = 60°$; (**d**) $\theta = 90°$; (**e**) $\theta = 0°$; (**f**) $\theta = 30°$; (**g**) $\theta = 60°$; (**h**) $\theta = 90°$.

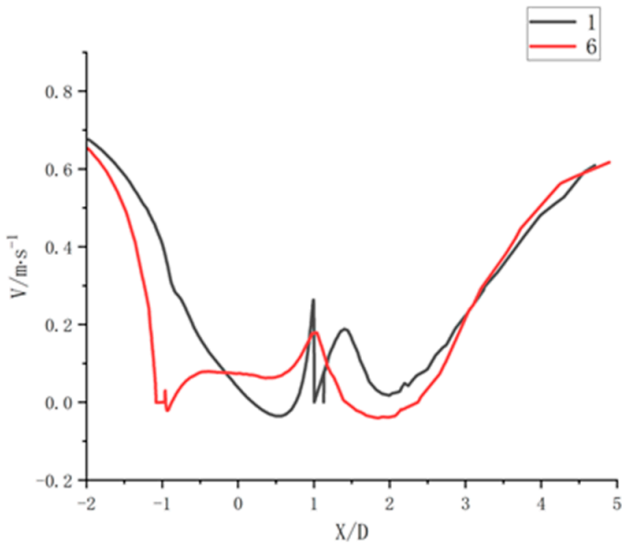

Figure 10. The flow velocity along the internal centerline within the turbine.

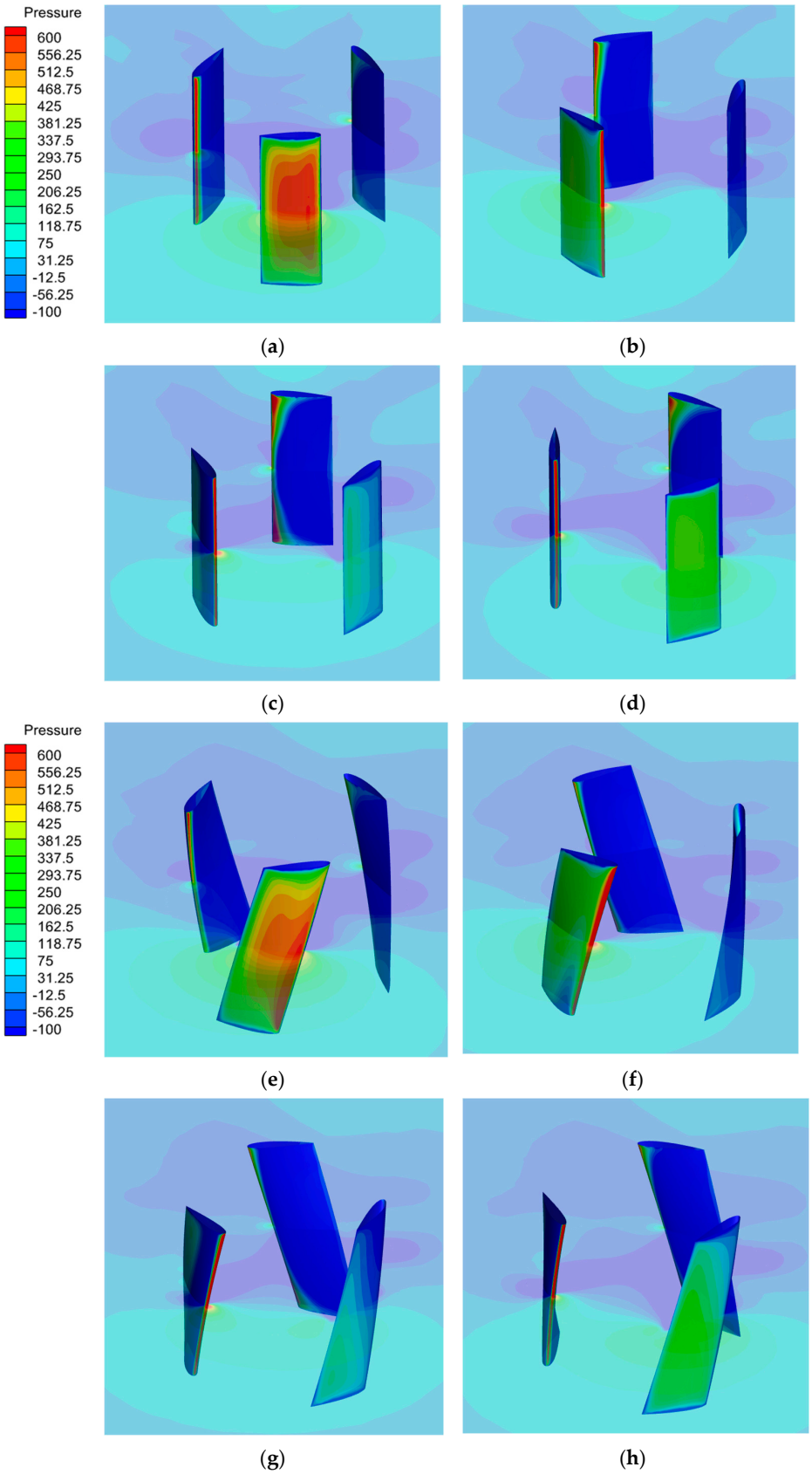

Figure 11. Pressure contour of turbine blades. (**a**) $\theta = 0°$; (**b**) $\theta = 30°$; (**c**) $\theta = 60°$; (**d**) $\theta = 90°$; (**e**) $\theta = 0°$; (**f**) $\theta = 30°$; (**g**) $\theta = 60°$; (**h**) $\theta = 90°$.

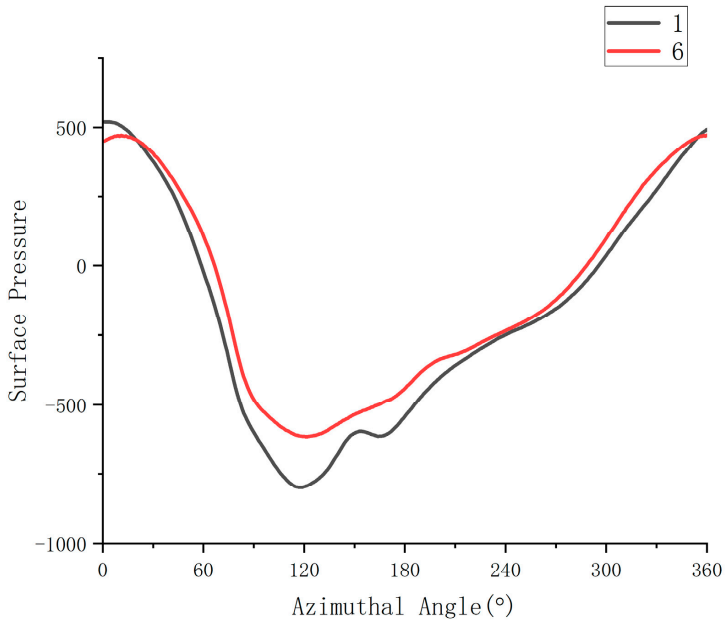

Figure 12. The pressure distribution on the windward surface of a single blade.

3.3. Analysis of Self-Starting Performance of Vertical Axis Turbines

The self-starting ability of a vertical-axis turbine refers to its capacity to generate starting torque at various azimuth angles. The larger the starting torque, the stronger the turbine's self-starting ability. Using the 6-DOF passive rotation method, the self-starting ability of NACA2418 with a 30° helical angle was compared to that of NACA0018 with a 0° helical angle under an incoming flow velocity of 0.8 m/s and optimal loading conditions that ensured maximum energy conversion efficiency for the turbines. The turbine's torque was converted into a torque coefficient according to Equation (2). Due to the symmetry of the vertical axis turbine, a self-starting analysis was conducted every 15°, resulting in 8 sets of data within the 0–120°.

These data were used to estimate the torque variation pattern over a complete rotation cycle, as shown in Figure 13. The NACA0018 turbine with a 0° helical angle exhibited significant fluctuations in starting torque within the 0–15°. The maximum starting torque coefficient was 0.26, occurring near the 90–105°, while the minimum value was 0.18, observed within the 0–45°. In contrast, the NACA2418 turbine with 30° helical angle exhibited smaller overall fluctuations in starting torque. The maximum starting torque coefficient was 0.25, occurring near 0–120°, while the minimum value was 0.20, located around 45°. Due to the 0° helicity of straight-blade vertical axis turbines when encountering water flow at different azimuth angles, the resulting torque fluctuations are significant. The minimum starting torque coefficient reflects the turbine's lowest starting capability [34]. The NACA2418 turbine with a 30° helical angle had a minimum starting torque coefficient of 0.20, which is higher than the 0.18 of the NACA0018 turbine with a 0°. This indicates that the 30° helical angle has better self-starting ability, with an improvement of 11.1%.

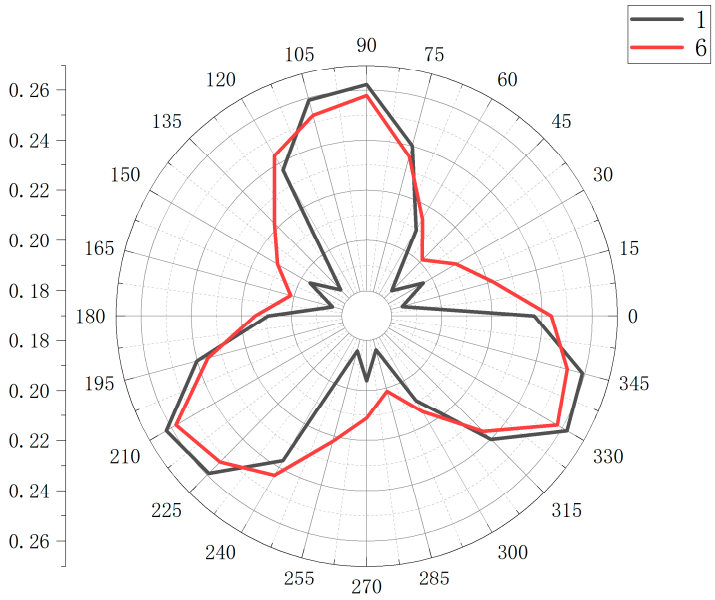

Figure 13. Self-starting torque coefficient of the turbine.

4. Experimental Validation and Analysis

The paper conducted experimental research and comparative analysis on vertical axis turbines with the same structure and operating conditions. The experimental model's overall structure utilized two shaftless brake discs at the top and bottom to support the turbine blades. The shaftless design avoids the impact of the secondary shaft connecting rod installation position (used to connect the main shaft and blades) on the overall performance of the turbine. The use of shaftless brake discs allows for precise adjustment of the blade pitch angle and improves the flow near the blade tips, preventing pressure leakage to the suction side of the blades. This helps to reduce tip vortices and spanwise flow. The upper and lower brake discs were manufactured using 3D printing technology with polylactic acid (PLA) material, which provides high strength and good rigidity, as shown in Figure 14a. The blades were also produced using 3D printing technology with photosensitive resin material, as shown in Figure 14b. The material enables extremely high printing precision, and the cured surface is very smooth, making it ideal for creating detailed models without the need for post-processing or surface finishing, as shown in Figure 14c.

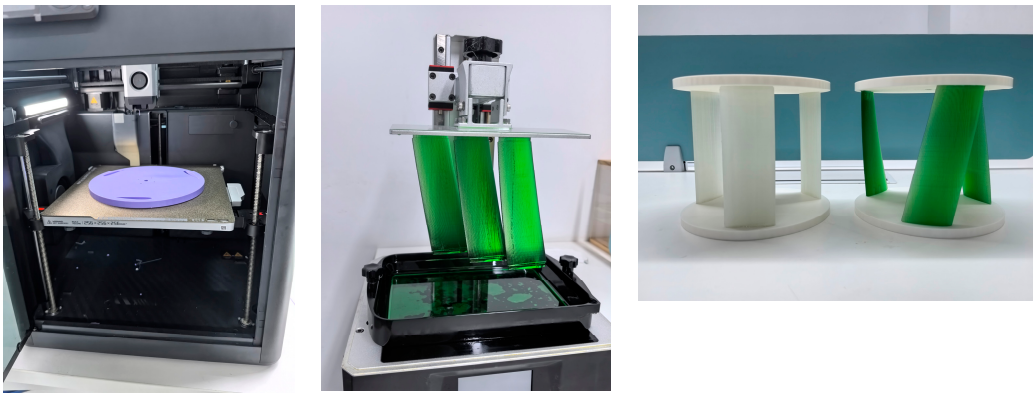

(**a**) (**b**) (**c**)

Figure 14. (**a**) The upper and lower brake discs; (**b**) 3D printing the blades; (**c**) Vertical Axis Hydrokinetic Turbine Model.

The NACA0018 symmetric airfoil as the initial airfoil (due to its symmetry, the thickness distributions of the upper and lower surfaces are identical, with a maximum thickness of 18% of the chord length, located at 0.3 chord length from the leading edge), a vertical-axis straight-bladed hydro turbine with 0-degree blade twist is selected as the control group. The NACA2418 asymmetric airfoil as the optimized airfoil (due to its asymmetry, the thickness distributions of the upper and lower surfaces differ, with a maximum thickness of 18% of the chord length and a maximum camber of 2% of the chord length located at 40% of the chord), a helical vertical-axis hydro turbine with a 30-degree blade twist (the projection of the airfoil cross-section at the blade tip onto the blade base plane forms a 30-degree angle) is selected as the experimental group, as shown in Table 4. Experimental validation of the simulation data is conducted in a recirculating water channel at a constant flow velocity of 0.8 m/s.

Table 4. Design parameters of the vertical-axis hydrokinetic turbine for the control group and the experimental group.

Structural Parameters	Control Group Values	Experimental Group Values
Blade Type	NACA0018	NACA2418
Diameter (D)	0.2 m	0.2 m
Number of blades (n)	3	3
Helicity (λ)	0°	30°
Blade chord length (C)	0.07 m	0.07 m
Blade height (H)	0.2 m	0.2 m
maximum thickness	18%	18%
maximum camber	0	2%

The experimental setup consists of a fixed frame, a vertical axis turbine, a torque sensor, a load, and a low-flow velocity measurement device, as shown in Figure 15. The non-contact dynamic torque sensor has a measuring range of 1 N/m, with an accuracy of less than 0.02%. It is connected to the turbine's rigid shaft via a flexible coupling.

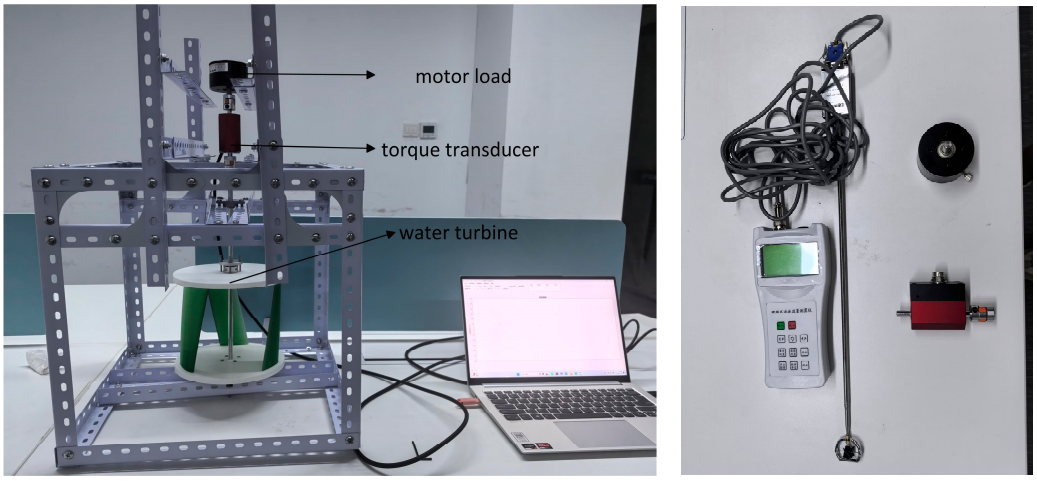

Figure 15. Experimental instruments.

The experiment utilized the research group's circulating water tank (as shown in Figure 16) to conduct low flow velocity tests on the vertical axis turbine. The specific parameters of the circulating water tank are detailed in Table 5.

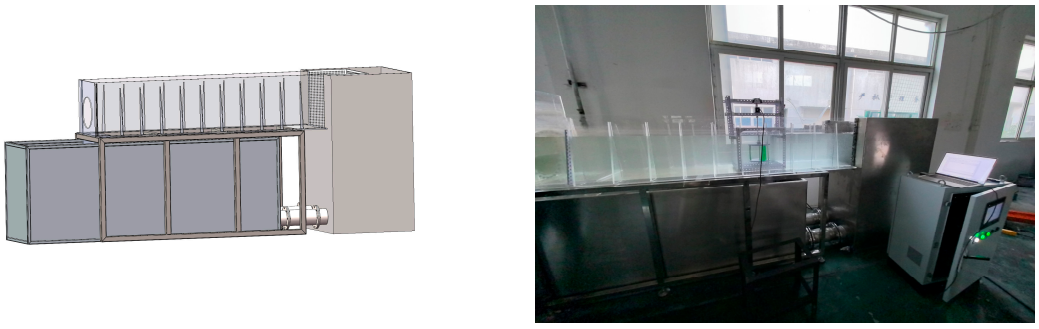

Figure 16. The recirculating water tank.

Table 5. The overall design parameters of the circulating water tank.

Structural Parameters	Values	Structural Parameters	Values
Flow Stabilizable box size (mm)	0800 × 1500 × 1000	Number of pumps	2
Tank thickness (mm)	5	Adjacent pump spacing (mm)	0.2 m
Water Flume length (mm)	2000	Inner diameter of pump outlet (mm)	150

The flow velocity in the rectangular experimental channel was controlled by adjusting the power of a submersible centrifugal pump. Flow velocity measurements in the turbine test area were taken using a low-flow velocity measuring device, with the vertical-axis hydro-kinetic turbine tested at a flow velocity of 0.8 m/s, as shown in Figure 17a. The vertical-axis turbine was installed in the front section of the rectangular test channel, maintaining a clearance of 0.05 m between the rotor brake disc and the channel bottom. Additionally, the turbine was positioned 0.10 m from the lateral boundaries and 0.15 m below the water surface. This setup minimized the influence of the experimental channel on the turbine's performance. Experiments were performed under various operating conditions to analyze changes in the power coefficient across a range of tip speed ratios (TSR). The experimental results are compared with the numerical simulation results, as shown in Figure 18a. The experimentally measured power coefficient demonstrates a strong correlation with the general trend of the numerically simulated power coefficient. Both values increase with the rise in TSR, reaching a peak above 1.2, and then decrease as TSR continues to rise. Overall, the numerical simulation results show strong consistency with the experimental data. To further validate the experimental error, the power of the submersible centrifugal pump was adjusted to maintain a consistent flow velocity of 0.8 m/s in the rectangular test channel for the vertical-axis turbine experimental setup. The load was adjusted to its optimal value, and six sets of stable maximum power for the vertical axis turbine were measured. The maximum error between the measured power coefficients and the numerical simulation results was 4.8%, as shown in Figure 18b.

The research primarily analyzes the performance of vertical-axis hydraulic turbines under low flow velocity conditions through numerical simulations, focusing on the effects of low flow velocity on power output and self-starting performance. The asymmetric airfoil features a highly curved upper surface that accelerates airflow, resulting in pressure reduction. This design generates significant lift at small angles of attack while maintaining favorable lift performance across a wide range of attack angles, thereby mitigating flow separation, vortex formation, and induced drag. The primary objective of the experimental work is to validate and verify the reliability of the simulation results. As the circulating

water channel test platform has certain limitations, the experimental research covers only a limited range of conditions. In practical applications, vertical-axis hydraulic turbines operate under various unsteady flow conditions that influence the parameters considered in the research. Future work will involve further refinement of experimental scope and parameter design to account for a broader range of operating conditions and to explore the underlying physical mechanisms of vertical-axis hydraulic turbines more comprehensively.

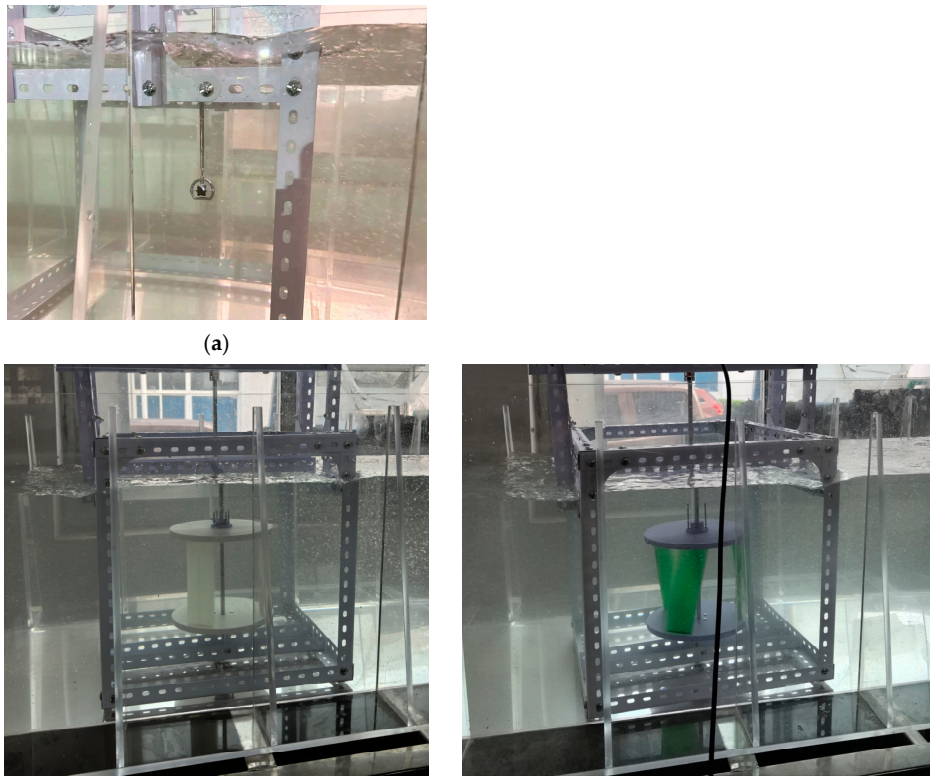

(**a**)

(**b**) (**c**)

Figure 17. Vertical axis hydrokinetic turbine at a flow velocity of 0.8 m/s. (**a**) The flow velocity measurements; (**b**) The NACA0018 turbine with a 0° helical angle; (**c**) The NACA2418 turbine with a 30° helical angle.

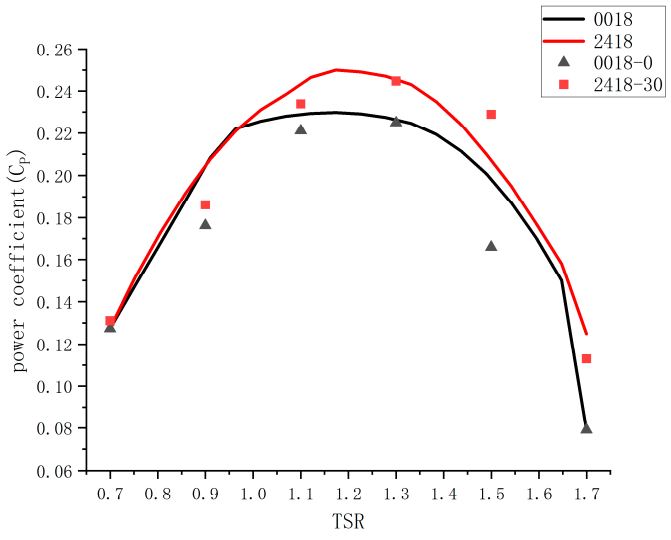

(**a**)

Figure 18. *Cont.*

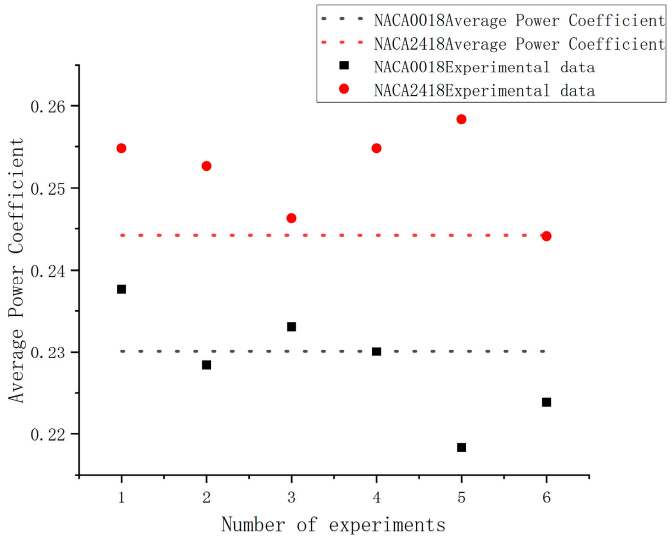

(**b**)

Figure 18. (**a**) The power coefficient at different tip speed ratios (TSR); (**b**) Comparison of the error between experimental average power and simulation data for the vertical axis turbine.

5. Conclusions

The paper investigates the effects of blade helical angle and airfoil curvature variation on the energy conversion efficiency and self-starting performance of vertical-axis hydraulic turbines under low flow velocity conditions through numerical simulations and experimental analysis. Given the relatively poor self-starting performance of straight-bladed vertical-axis hydraulic turbines in low flow velocities, a helical blade design is proposed to enhance self-starting capability. Additionally, the traditional symmetric airfoil is replaced with an asymmetric airfoil to improve energy capture efficiency. The results demonstrate that optimizing airfoil curvature and adjusting the blade helical angle can significantly enhance the hydrodynamic performance of vertical-axis hydraulic turbines. Comparative analysis with conventional straight-bladed vertical-axis hydraulic turbines further validates the effectiveness of these design improvements.

The helical blades improve energy conversion efficiency by reducing the generation of tip vortices, decreasing lateral torque fluctuations, and enhancing the overall stability of the turbine. Compared to the initial symmetric airfoil with 0° helical blades, the optimized vertical axis turbine with 20% curvature asymmetric airfoil and 30° helical blades achieved a 6.13% increase in energy conversion efficiency. The initial turbine power coefficient was 0.2301, which improved to 0.2442 in the optimized design. However, further increasing the curvature and helical angle leads to a reduction in energy conversion efficiency, indicating that excessive twist angles may negatively impact hydrokinetic performance. The turbine power coefficient for 30° and 60° helical blades was below 0.1.

Helical blades exhibit a greater self-starting advantage at low flow velocity conditions. The minimum self-starting torque coefficient of the turbine was improved from 0.18 in the initial design to 0.20 in the optimized design, representing an 11.1% increase. The helicity allows for a more uniform distribution of the blades around the rotating cylinder, reducing the lateral torque fluctuations, with the fluctuation rate decreasing by 32.14%. The initial power coefficient fluctuation of the turbine was 94.74%, which decreased to 64.29% after the improvements. The results provide a valuable reference for optimizing the design of vertical axis turbines under low-flow velocity conditions.

Author Contributions: Conceptualization, Y.H. and C.S.; Methodology, Y.H. and C.S.; Formal analysis Y.H., C.S., Z.W. and S.W.; Data curation, Y.H.; Software, Y.H.; Writing—original draft preparation, Y.H. and C.S.; Writing—review and editing, Y.H.; Supervision, C.S., Z.W. and S.W.; Project administration, C.S., Z.W. and S.W. All authors have read and agreed to the published version of the manuscript.

Funding: This research was funded by 2024 Shanghai University Teachers Industry-University-Research Practice Program (A1-2007-24-000405), 2024 Shanghai Science and Technology Innovation Action Plan Soft Science Research Project (24692113800), 2024 Hainan Tropical Marine Aquaculture Technology Key Laboratory Open Project (HNTMTOF202404).

Data Availability Statement: The data presented in this study are available on request from the corresponding author. The data are not publicly available due to privacy.

Conflicts of Interest: The authors declare no conflicts of interest.

Nomenclature

The following abbreviations are used in this manuscript:

TSR	Tip speed ratio (ω *R/V*)
H	Height of turbine [m]
D	Diameter of turbine [m]
R	Radius of turbine [m]
C	Chord length [m]
A	Swept area ($D \times H$) [m^2]
C_P	Power coefficient
$C_{P\max}$	Maximum power coefficient in unit period
$C_{P\min}$	Minimum power coefficient in unit period
C_M	Torque coefficient
ω	Rotational angular velocity [rad/s]
σ	Solidity ratio
V	Free stream water velocity [m/s]
V_0	Incoming flow velocity [m/s]
ρ	Density of water [kg/m^3]
VAHT	Vertical axis hydrokinetic turbine
λ	Blade helicity
n	Number of blades
α	Projection angle [°]
β	Pitch angle [°]
T	Total torque
f	load torque
$\overline{C_P}$	Average power coefficient
δ	Instability of power coefficient
GCI	Grid Convergence Index
CFD	Computational fluid dynamics

References

1. Laws, N.D.; Epps, B.P. Hydrokinetic energy conversion: Technology, research, and outlook. *Renew. Sustain. Energy Rev.* **2016**, *57*, 1245–1259. [CrossRef]
2. Khan, M.; Bhuyan, G.; Iqbal, M.; Quaicoe, J. Hydrokinetic energy conversion systems and assessment of horizontal and vertical axis turbines for river and tidal applications: A technology status review. *Appl. Energy* **2009**, *86*, 1823–1835. [CrossRef]
3. Kirke, B.; Lazauskas, L. Limitations of fixed pitch Darrieus hydrokinetic turbines and the challenge of variable pitch. *Renew. Energy* **2011**, *36*, 893–897. [CrossRef]
4. Saini, G.; Saini, R.P. A review on technology, configurations, and performance of cross-flow hydrokinetic turbines. *Int. J. Energy Res.* **2019**, *43*, 6639–6679. [CrossRef]

5. Vu, N.A.; Pham, N.S. An Analytical Methodology for Aerodynamic Analysis of Vertical Axis Wind Turbine. *Int. J. Renew. Energy Res.* **2020**, *10*, 1145–1153.
6. Ma, Y.; Hu, C.; Li, Y.; Li, L.; Deng, R.; Jiang, D. Hydrodynamic performance analysis of the vertical axis twin-rotor tidal current turbine. *Water* **2018**, *10*, 1694. [CrossRef]
7. Yosry, A.G.; Fernández-Jiménez, A.; Álvarez-Álvarez, E.; Marigorta, E.B. Design and characterization of a vertical-axis micro tidal turbine for low velocity scenarios. *Energy Convers. Manag.* **2021**, *237*, 114144. [CrossRef]
8. Chen, D.; Ma, Y.; Hu, C.; Zhao, T. Efficiency optimization of twin vertical-axis helical hydrokinetic turbines (VAHHTs) based on Taguchi method. *Appl. Ocean Res.* **2023**, *138*, 103618. [CrossRef]
9. Singh, M.; Biswas, A.; Misra, R. Investigation of self-starting and high rotor solidity on the performance of a three S1210 blade H-type Darrieus rotor. *Renew. Energy* **2015**, *76*, 381–387. [CrossRef]
10. Castelli, M.R.; Englaro, A.; Benini, E. The Darrieus wind turbine: Proposal for a new performance prediction model based on CFD. *Energy* **2011**, *36*, 4919–4934. [CrossRef]
11. Divakaran, U.; Ramesh, A.; Mohammad, A.; Velamati, R.K. Effect of helix angle on the performance of helical vertical axis wind turbine. *Energies* **2021**, *14*, 393. [CrossRef]
12. Bayram, A.; Dhalwala, M.; Oshkai, P.; Korobenko, A. Numerical simulations of a vertical-axis hydrokinetic turbine with different blade-strut configurations under free-surface effects. *Eng. Comput.* **2023**, *39*, 1041–1054. [CrossRef]
13. Satrio, D.; Ramadhan, L.I. The advantage of flow disturbance for vertical-axis turbine in low current velocity. *Sustain. Energy Technol. Assess.* **2022**, *49*, 101692. [CrossRef]
14. Khan, F.; Sheikh, S.R.; Masud, J. Behavior Analysis of Vertical Axis Water Turbine with Individual Blade Pitch Control. In Proceedings of the AIAA SCITECH 2023 Forum, National Harbor, MD, USA, 23–27 January 2023; p. 2174.
15. Yosry, A.G.; Álvarez, E.Á.; Valdés, R.E.; Pandal, A.; Marigorta, E.B. Experimental and multiphase modeling of small vertical-axis hydrokinetic turbine with free-surface variations. *Renew. Energy* **2023**, *203*, 788–801. [CrossRef]
16. Abdolahifar, A.; Azizi, M.; Zanj, A. Flow structure and performance analysis of Darrieus vertical axis turbines with swept blades: A critical case study on V-shaped blades. *Ocean Eng.* **2023**, *280*, 114857. [CrossRef]
17. Bachant, P.; Wosnik, M. Performance measurements of cylindrical-and spherical-helical cross-flow marine hydrokinetic turbines, with estimates of exergy efficiency. *Renew. Energy* **2015**, *74*, 318–325. [CrossRef]
18. Zhang, G.; Yang, Y.; Chen, J.; Jin, Z.; Dykas, S. Numerical study of heterogeneous condensation in the de Laval nozzle to guide the compressor performance optimization in a compressed air energy storage system. *Appl. Energy* **2024**, *356*, 122361. [CrossRef]
19. Alam, M.J.; Iqbal, M.T. Design and development of hybrid vertical axis turbine. In Proceedings of the Conference on Electrical & Computer Engineering, St. John's, NL, Canada, 3–6 May 2009.
20. Basumatary, M.; Biswas, A.; Misra, R.D. CFD study of a combined lift and drag-based novel Savonius vertical axis water turbine. *J. Mar. Sci. Technol.* **2023**, *28*, 27–43. [CrossRef]
21. Khan, Z.U.; Ali, Z.; Uddin, E. Performance enhancement of vertical axis hydrokinetic turbine using novel blade profile. *Renew. Energy* **2022**, *188*, 801–818. [CrossRef]
22. Satrio, D.; Utama, I.K.A.P. Experimental investigation into the improvement of self-starting capability of vertical-axis tidal current turbine. *Energy Rep.* **2021**, *7*, 4587–4594. [CrossRef]
23. Talukdar, P.K.; Kulkarni, V.; Dehingia, D.; Saha, U.K. Evaluation of a model helical bladed hydrokinetic turbine characteristics from in-situ experiments. In Proceedings of the ASME 2017 11th International Conference on Energy Sustainability, Charlotte, NC, USA, 26–30 June 2017; p. V001T007A005.
24. Pongduang, S.; Kayankannavee, C.; Tiaple, Y. Experimental Investigation of Helical Tidal Turbine Characteristics with Different Twists. *Energy Procedia* **2015**, *79*, 409–414. [CrossRef]
25. Ma, Y.; Zhu, Y.; Zhang, A.; Hu, C.; Liu, S.; Li, Z. Hydrodynamic performance of vertical axis hydrokinetic turbine based on Taguchi method. *Renew. Energy* **2022**, *186*, 573–584. [CrossRef]
26. Shen, C.; Zhang, J.; Ding, C.; Wang, S. Simulation Analysis and Experimental Study on Airfoil Optimization of Low-Velocity Turbine. *J. Mar. Sci. Eng.* **2024**, *12*, 303. [CrossRef]
27. Yang, B.; Shu, X.W. Hydrofoil optimization and experimental validation in helical vertical axis turbine for power generation from marine current. *Ocean Eng.* **2012**, *42*, 35–46. [CrossRef]
28. Khanjanpour, M.H.; Javadi, A. Optimization of the hydrodynamic performance of a vertical Axis tidal (VAT) turbine using CFD-Taguchi approach. *Energy Convers. Manag.* **2020**, *222*, 113235. [CrossRef]
29. Sengupta, A.R.; Biswas, A.; Gupta, R. Studies of some high solidity symmetrical and unsymmetrical blade H-Darrieus rotors with respect to starting characteristics, dynamic performances and flow physics in low wind streams. *Renew. Energy Int. J.* **2016**, *93*, 536–547. [CrossRef]
30. Brusca, S.; Lanzafame, R.; Messina, M. Design of a vertical-axis wind turbine: How the aspect ratio affects the turbine's performance. *Int. J. Energy Environ. Eng.* **2014**, *5*, 333–340. [CrossRef]

31. Wang, X.; Luo, X.; Zhuang, B.; Yu, W.; Xu, H. 6-DOF Numerical Simulation of the Vertical-Axis Water Turbine. In Proceedings of the ASME-JSME-KSME 2011 Joint Fluids Engineering Conference, Hamamatsu, Japan, 24–29 July 2011.
32. Talukdar, P.K.; Kulkarni, V.; Saha, U.K. Field-testing of model helical-bladed hydrokinetic turbines for small-scale power generation. *Renew. Energy* **2018**, *127*, 158–167. [CrossRef]
33. Zhang, G.J.; Li, Y.P.; Jin, Z.L.; Dykas, S. Prediction of the non-equilibrium condensation characteristic of CO_2 based on a Laval nozzle to improve carbon capture efficiency. *Fuel* **2025**, *381*, 133303. [CrossRef]
34. Rivera, M.; Shook, D.; Foust, E. Experimental and Numerical Investigation into Vertical Axis Water Turbine Self-Starting Phenomenon. In Proceedings of the ASME 2020 International Mechanical Engineering Congress and Exposition, Virtual, 16–19 November 2020.